American Mineralogist, Volume 111, pages 903–910, 2026

Grahampearsonite, $Ca_2P_2O_7$, a new mineral found in a super-deep diamond from Juína, Brazil

Yanjuan Wang[1,2,‡], Fabrizio Nestola[2,*,†], Maxwell C. Day[2,§], Tiago Jalowitzki[3], Eduardo Novais Rodrigues[2], Fernanda Gervasoni[4,5], Daniel Grings Cedeño[5], Sebastião William da Silva[6], Reinhardt Adolfo Fuck[3], Jacopo Nava[2], Lisa Santello[2], Martha G. Pamato[2], Davide Novella[2], Francesca Innocenzi[2], Andrea Curtolo[2,7], Mattia La Fortezza[2], and Kai Qu[8,9,‖]

[1]State Key Laboratory of Deep Earth and Mineral Exploration, Chinese Academy of Geological Sciences, Beijing 100037, China
[2]Department of Geosciences, University of Padova, 35131 Padua, Italy
[3]Universidade de Brasília, Instituto de Geociências, Programa de Pós-graduação em Geologia, 70910-900 Brasília, DF, Brazil
[4]Brazilian Synchrotron Light Laboratory, Brazilian Center for Research in Energy and Materials (LNLS/CNPEM), Campinas, 13083-100, Brazil
[5]Programa de Pós-graduação em Geociências, Universidade de Federal do Rio Grande do Sul (UFRGS), Porto Alegre, 91501-970, Brazil
[6]Instituto de Física, Universidade de Brasília (UnB), Brasília, 70910-900, Brazil
[7]Bayerisches Geoinstitut, Universität Bayreuth, 95440, Bayreuth, Germany
[8]Tianjin Centre, China Geological Survey, Tianjin 300170, China
[9]School of Earth Sciences and Engineering, Nanjing University, Xixia, Nanjing 210023, China

Abstract

Grahampearsonite, ideally $Ca_2P_2O_7$, is a new mineral (IMA 2025-017) that was found in a multiphase inclusion in a super-deep diamond (sample RV43) from the Chapadão plateau, Mato Grosso, Brazil. The new mineral is closely associated with tuite and with other mineral inclusions in the host diamond (that are not in direct contact with grahampearsonite) including larnite, merrillite, apatite, diopside, ilmenite, magnetite, calcite, and an unidentified phosphate phase. X-ray diffraction analyses, performed directly on the inclusion while still entrapped in the diamond, revealed a tetragonal crystal structure (space group $P4_1$), with unit-cell parameters $a = 6.6966(16)$ Å, $c = 24.145(11)$ Å, and $V = 1082.8(6)$ Å^3. The identification of grahampearsonite as the natural analog of synthetic β-$Ca_2P_2O_7$ is strongly supported by micro-Raman, FTIR, crystal chemical, and X-ray diffraction data. The occurrence of grahampearsonite and tuite in a super-deep diamond indicates that grahampearsonite could be related to the decomposition of tuite and may provide new insights into the Earth's deep phosphorus reservoir and the crust-mantle phosphorus cycle. The new mineral honors Graham D. Pearson, University of Alberta, for his outstanding contributions to diamond research.

Keywords: Gramhampearsonite, tuite, super-deep diamond, new mineral, phosphate, Brazil

Introduction

Super-deep diamonds (SDDs) form at depths exceeding 300 km and serve as chemically inert and physically robust time-capsules that preserve high-pressure mineral inclusions, providing exceptional insights into the composition and dynamics of Earth's deep interior (Lorenzon et al. 2023, Day et al. 2023; Genzel et al. 2023; Shirey et al. 2024). Diamonds from the Juína region in Brazil contain various mineral inclusions such as ferropericlase, majoritic garnet, and bridgmanite (retrogressed), indicative of lower mantle to transition zone conditions (Anzolini et al. 2019). Of most importance was the discovery of a ringwoodite inclusion (containing ~1.4 wt% H_2O) in a Juína diamond, indicating the hydrous nature of the transition zone (Pearson et al. 2014). These inclusions are essential for elucidating the deep geochemical cycling of elements and for constraining the pressure-temperature environments of diamond formation.

Phosphate minerals are relatively uncommon among inclusions in diamonds (Smith et al. 2022). Apatite has been reported as a rare inclusion in cratonic diamonds, yet its paragenesis remains uncertain (Stachel et al. 2022). Despite this, observations of apatite accord with observations of other high-pressure phosphates, for example, tuite [ideally $Ca_3(PO_4)_2$], a high-pressure polymorph of apatite (Konzett and Frost 2009; Zhang et al. 2026). Moreover, Kaminsky and Zedgenizov (2022) reported merrillite in a lower-mantle diamond, but it is unclear exactly how merrillite [ideally $Ca_9NaMg(PO_4)_7$] forms, with some options involving formation due to prograde transformation of apatite or retrograde transformation of tuite. Apart from the orthophosphates [containing $(PO_4)^{3-}$ groups] mentioned above, two pyrophosphates [containing $(P_2O_7)^{4-}$ groups] have been identified in a

* Corresponding author E-mail: fabrizio.nestola@unipd.it Orcid https://orcid.org/0000-0002-4875-5125

‡Orcid https://orcid.org/0000-0002-6985-2012
§Orcid https://orcid.org/0000-0002-3295-2116
‖Orcid https://orcid.org/0000-0002-4961-9598

0003-004X/26/0006–903$05.00/DOI: https://doi.org/10.2138/am-2025-10072

diamond from the Juína area (Brazil), $Na_4Mg_3(PO_4)_2(P_2O_7)$ and $Fe_2Fe_5(P_2O_7)_4$ (Kaminsky et al. 2013).

Phosphorus is a moderately incompatible element whose behavior in the mantle is strongly influenced by redox conditions and volatile activity. It is mainly sourced from phosphates, which serve as important reservoirs for volatiles (e.g., OH^-, F^-, Cl^-) and trace elements, including rare earth elements, U, Th, and Sr. The observation of phosphate inclusions in SDDs may provide insights into the deep subduction of oceanic crust, the production of associated carbonatitic melts, and the subsequent cycling of volatiles, carbon (C) and incompatible elements, like P, in the deep mantle. Several studies have shown that significant quantities of P may be incorporated into silicates via Si → P substitution, implying that nominally anhydrous silicates (e.g., majoritic garnet) can store P at mantle conditions (Pausch et al. 2024). However, the dominant mineral hosts of P at different *P*/*T* conditions in the mantle remain poorly constrained.

Before the discovery of grahampearsonite in this study, no Ca-pyrophosphate had been observed in diamond and only five Ca-bearing pyrophosphate minerals are currently known in nature (i.e., anastasenkoite, canaphite, lisanite, shasuite, and wooldridgeite). Nevertheless, Ca-pyrophosphates have been extensively studied in synthetic systems and technical applications (Miller and Parris 1964; Bian et al. 2003, 2004; Gras et al. 2013; Elbashir et al. 2024). The synthetic Ca pyrophosphate phase, ideally $Ca_2P_2O_7$, plays an important role in applications within the fields of luminescence and biomaterials (Ranby et al. 1955; Lin et al. 1995; Bian et al. 2004). The crystal structure of $Ca_2P_2O_7$ has been extensively studied at room pressure and three polymorphs of this Ca pyrophosphate are known: α-$Ca_2P_2O_7$ which forms at ~1140–1220 °C with $P2_1/n$ symmetry; β-$Ca_2P_2O_7$ which forms at ~750–1140 °C with $P4_1$ symmetry; and γ-$Ca_2P_2O_7$, which forms below 750 °C with $P\bar{1}$ symmetry (Webb 1966; Calvo 1968; Boudin et al. 1993; Sauskojus et al. 2022).

Here we report a natural analog of synthetic β-$Ca_2P_2O_7$, grahampearsonite, found in a SDD from Juína, Brazil. The phase and the name have been approved by the Commission on New Minerals, Nomenclature and Classification of the International Mineralogical Association (IMA-CNMNC) with number IMA 2025-017. It is named in honor of Graham D. Pearson (Fig. 1), born in 1965, a British geologist and geochemist, for his outstanding contributions using isotopic tracers on diamonds and mantle peridotites to understand the composition and evolution of the mantle roots underpinning continents and the deep interior of the Earth. The holotype material is deposited at the Museum of Nature and Humankind (University of Padova, Corso Giuseppe Garibaldi, 39, 35121 Padova, Italy) with the catalog number of MMP M23231.

Occurrence and Paragenesis

The mineral grahampearsonite was found as an inclusion in a SDD (RV43) from Brazil (11°26′52.37″S and 58°56′12.20″W). Sample RV43 was donated by Romeu Veronese (R.V.), who is the owner of the property where industrial diamonds are prospected from a strongly weathered kimberlite (primary source). This locality is situated in the Chapadão plateau (U-Pb age of 93.6 ± 0.4 Ma), previously named Pandrea, in the Juína kimberlite field (Cabral-Neto et al. 2024). The Chapadão kimberlite cluster, within the Juína Field, is composed of crater-facies kimberlites containing ash-fall and/or tuffisitic material, which are covered by Upper Cretaceous and Tertiary sediments (Kaminsky et al. 2010). The kimberlitic indicator minerals are spinel, picroilmenite, manganoan ilmenite, and zircon. The diamond samples are preferentially concentrated in white layers that represent weathered pyroclastic fragments.

Figure 1. Photo of Graham D. Pearson doing fieldwork in Ellesmere Island, Canada (right) and in the Juína region, Brazil (left) where the diamond containing grahampearsonite was discovered.

Grahampearsonite occurs as a mineral inclusion in diamond RV43 (Fig. 2) and is closely associated with tuite (Fig. 3). However, these two phases do not show any specific common crystallographic orientation (evaluated by single-crystal X-ray diffraction). Other mineral inclusions in the host diamond (but not in direct contact with grahampearsonite) include larnite, merrillite, apatite, diopside, ilmenite, magnetite, calcite, and another unknown phosphate phase that has yet to be identified. Grahampearsonite occurs as subhedral granular crystals ~3–20 μm in size. A density of 3.107 g/cm^3 is calculated based on the empirical formula and unit-cell volume refined from single-crystal X-ray diffraction (XRD) data. Other physical properties could not be determined due to the small crystal size and the nature of the sample entrapped in the diamond host. However, such properties are expected to be similar to synthetic β-$Ca_2P_2O_7$.

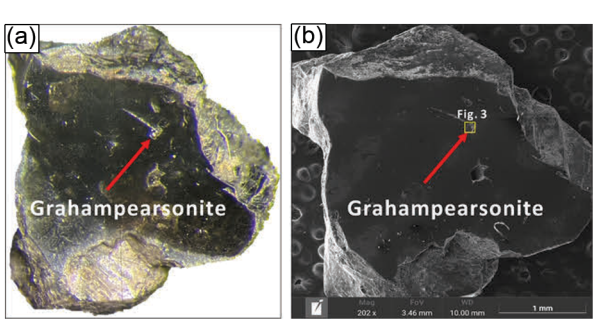

Figure 2. Mineral inclusion of grahampearsonite exposed on the polished surface of diamond RV43. (**a**) Stereo-microscope image. (**b**) SEM-BSE image [the inset in (**b**) is magnified in Fig. 3].

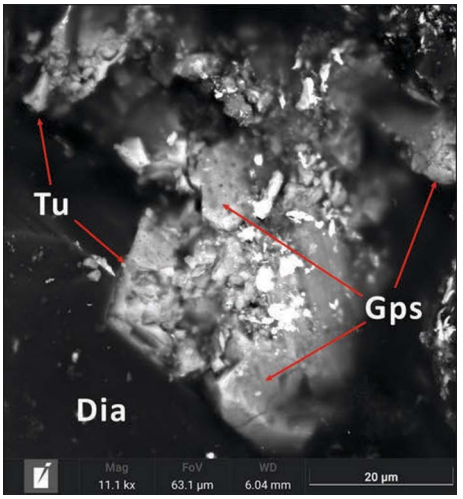

FIGURE 3. SEM-BSE image of grahampearsonite associated with tuite comprising an inclusion inside diamond RV43. Gps = grahampearsonite; Tu = tuite; Dia = diamond. Mineral abbreviations are from Warr (2021).

METHODS

Fourier-Transform Infrared Spectroscopy

Fourier-transform infrared spectroscopic (FTIR) analysis of grahampearsonite was performed at the Department of Geosciences, University of Padova (Italy), using a Thermo Fisher Nicolet iN10 InfraRed microscope equipped with a KBr beam splitter and a LN-cooled MCT detector. The spectrum of grahampearsonite (Fig. 4) was collected at an operating resolution of 4 cm^{-1} over the range 4000–750 cm^{-1} by averaging 64 scans with a scan time of 22.4 s. In preparation for FTIR analysis, the sample was cleaned and mounted on a BaF_2 background window. Raw spectra were baseline-corrected using the OMNIC spectra software.

Raman Spectroscopy

Micro-Raman analyses were performed at the Department of Geosciences, University of Padova (Italy), using a WITec alpha300 R Raman Imaging Microscope equipped with a green laser (532 nm). Analyses were conducted using a 50× long working distance objective with 2.5 cm^{-1} spectral resolution and spectra were recorded over the range 100 to 3850 cm^{-1}. The spectrum was accumulated 10 times using an integration time of 20 s. The Raman instrument was calibrated with a silicon plate for intensity and peak position of the 520 cm^{-1} silicon band. Raman data were treated using the RamanCrystalHunter software (RCH, Nestola et al. 2025).

Chemical Composition

Quantitative chemical analyses of grahampearsonite were determined using a Tescan Solaris Field-Emission SEM at the Department of Geoscience at the University of Padova using a WDS-EDS integrated system. This instrument is equipped with a high-resolution Ultim max 65 Oxford Instruments silicon-drift EDS detector. The operating conditions were 15 keV accelerating voltage, 3 nA beam current, and a 1 µm beam diameter with a working distance of 5 mm. The WDS-EDS system was standardized using the following natural minerals and synthetic oxides: Amelia plagioclase (Si, Na), diopside (Ca), San Carlos olivine (Mg), iron oxide (Fe), orthoclase (K), Durango apatite (P), and barite (S). The current was calibrated using a cobalt reference, and a ZAF correction, built into the Oxford AzTec software, was applied.

Single-Crystal X-ray Diffraction

Since it was not possible to safely extract the grains of grahampearsonite (and/or tuite) from the host diamond, due to the tendency of inclusions within diamonds to break upon their release, the entire mineral assemblage was centered directly under the X-ray beam while still inside the diamond (as typically done during non-destructive X-ray diffraction analysis of inclusions in diamonds) (Angel et al. 2022). The single-crystal X-ray diffraction analysis was performed using a Rigaku Oxford Diffraction SuperNova diffractometer equipped with a Dectris Pilatus 200K area detector and a Mo$K\alpha$ X-ray micro-source at the Department of Geosciences, University of Padova (Italy). The instrument was controlled using the CrysAlisPro software (Rigaku). The sample-to-detector distance was set to 69 mm, and the X-ray beam at the sample position was 120 µm. The working conditions were 50 kV and 0.12 mA. The data were collected over 287 frames and 7 runs, with an exposure time of 200 s per rotation degree, for a total data collection time of 15 h and 29 min.

RESULTS

FTIR Spectroscopy

The spectrum of grahampearsonite was collected through the host diamond, which resulted in characteristic diamond absorption from 1600 to 3800 cm^{-1} (Fig. 4a). Although nitrogen (N) impurities in diamond can produce signal from 1100 to 1400 cm^{-1}, no peaks due to N were observed anywhere near the inclusion of grahampearsonite (the diamond is *Type IIa*) and thus we can confirm that the signal observed in this region (Fig. 4b) is only due to grahampearsonite. Two weak peaks are observed at 2926 and 2854 cm^{-1} due to surface contamination (grease), and regions with relatively more noise observed at 3975–3540 and 1565–1430 cm^{-1} are due to atmospheric contamination by H_2O vapor.

The FTIR spectrum of grahampearsonite (Fig. 4b) is almost identical to the spectrum of synthetic $Ca_2(P_2O_7)$ (NIST Standard Reference Database 69) and is very similar to the spectra of other metal pyrophosphates (e.g., Petrova et al. 1995; Bih et al. 2006; Kohale and Dhoble 2012, 2018; Sronsri and Boonchom 2018; Baitahe et al. 2022). Moreover, individual peak positions and their assignment to particular vibrational modes are in excellent agreement with those reported by Cornilsen and Condrate (1979). The signal at ~950 cm^{-1} is characteristic of $(P_2O_7)^{4-}$ groups and is attributed to asymmetric stretching modes of the P-O-P bridge [ν_{as}(P-O-P)] (Sronsri and Boonchom 2018). Bands observed in the 1000 to 1070 cm^{-1} and 1120 to 1230 cm^{-1} ranges are attributed to $\nu_{as}(PO_3)$ modes, and bands observed in the 1070 to 1120 cm^{-1} range are attributed to $\nu_s(PO_3)$ modes (Cornilsen and Condrate 1979; Baitahe et al. 2022).

Micro-Raman Spectroscopy

The Raman spectrum of grahampearsonite is practically identical to the spectrum of the synthetic β-$Ca_2P_2O_7$ (Cornilsen and Condrate 1979; Baitahe et al. 2022) (Fig. 5). Almost all peaks in the Raman spectrum of β-$Ca_2P_2O_7$, in the 100–1200 cm^{-1} region, are observed in the spectrum of grahampearsonite, and their relative intensities are similar. The $(P_2O_7)^{4-}$ anion can be expressed as $(O_3P\text{-}O\text{-}PO_3)^{4-}$, where asymmetric and symmetric vibrational modes of PO_3 groups and P-O-P (and O-P-O) bridges produce characteristic bands in the Raman and infrared spectra (Corbridge 1966). These different vibrational modes produce several peaks across particular frequency ranges (see FTIR section above). The most intense Raman band observed at 1047 cm^{-1} is attributed to asymmetric stretching of the PO_3 group [$\nu_{as}(PO_3)$]. Additional relatively weaker peaks in the 1000–1180 cm^{-1} range are attributed to asymmetric and symmetric stretching modes of PO_3 groups ([$\nu_{as}(PO_3)$] and [$\nu_s(PO_3)$], respectively) (Baitahe et al. 2022). The peak at 736 cm^{-1} is a characteristic feature of the

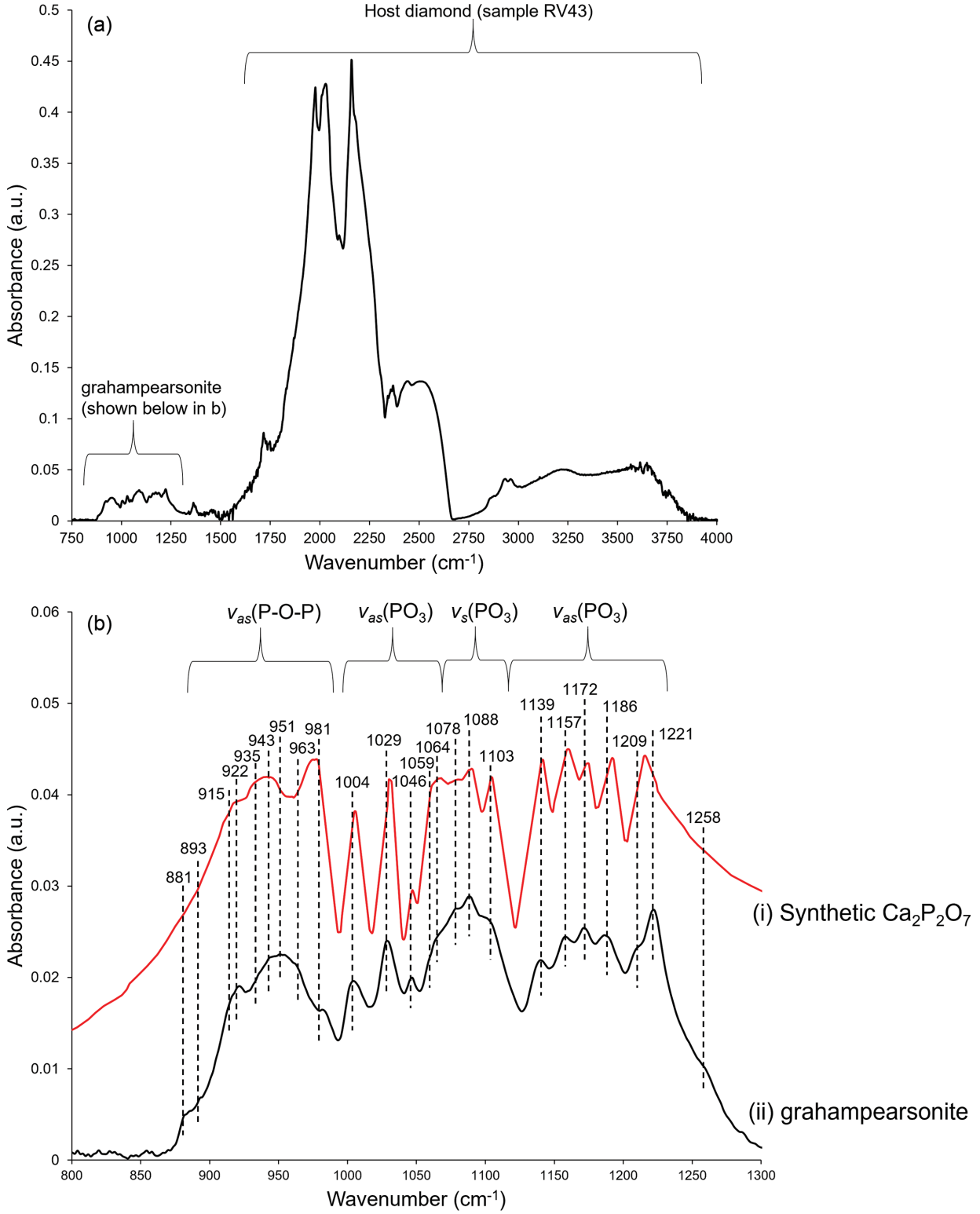

Figure 4. FTIR spectra of (**a**) grahampearsonite (800 to 1300 cm^{-1}) and the surrounding host diamond (1600 to 3800 cm^{-1}), and (**b**) grahampearsonite and its synthetic $Ca_2P_2O_7$ analog (from NIST Standard Reference Database 69), where all bands are assigned to different vibrational modes of the $(P_2O_7)^{4-}$ group.

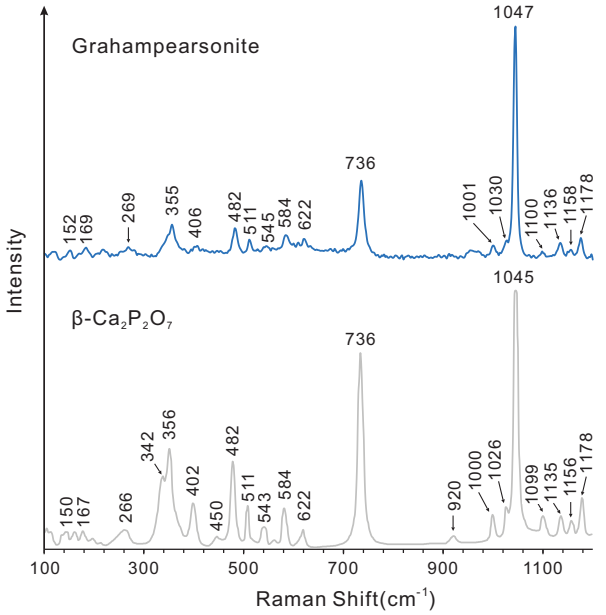

Figure 5. Raman spectrum of grahampearsonite (on the top in blue) [processed by RamanCrystalHunter (RCH) software (Nestola et al. 2025)] and synthetic β-$Ca_2P_2O_7$ (on the bottom in gray, taken from Baitahe et al. 2022).

$(P_2O_7)^{4-}$ anion and corresponds to symmetric stretching of the P-O-P bridge [ν_s(P-O-P)] (Sronsri and Boonchom 2018). Relatively weak bands from ~270–620 cm^{-1} are attributed to: (1) bending of O-P-O bridges; (2) bending (and/or deformation) modes of PO_3 groups; and/or (3) Ca-O vibrational modes. Bands below ~260 cm^{-1} are attributed to Ca-O vibrational modes and intrinsic lattice vibrations (Baitahe et al. 2022).

Chemical Composition

The compositional data from seven analysis points are provided in Table 1. The empirical chemical formula is: $(Ca_{1.92}Fe_{0.03}Mg_{0.01}Na_{0.01})_{\Sigma 1.97}(P_{1.99}Si_{0.01}S_{0.01})_{\Sigma 2.01}O_7$. The ideal end-member formula is $Ca_2P_2O_7$, which requires CaO 44.14 and P_2O_5 55.86, total 100 wt%. The analyses were performed on the available surfaces of grahampearsonite, which was exposed during the diamond polishing

X-ray Crystallography and Structure Determination

Using the procedure described in the Methods section, we collected a total of 988 diffraction reflections from grahampearsonite. These 988 reflections are from the entire mineral assemblage, including the diamond host. The data provided the unit cell of the diamond host [a = 3.614(10) Å, V = 47.2(2) $Å^3$], an additional 141 reflections provided the unit cell of tuite [hexagonal cell with a = 5.255(2) Å, c = 18.685(12) Å, V = 446.9(4) $Å^3$]; finally, 156 reflections provided the tetragonal unit-cell of grahampearsonite:

$a = 6.6966(16)$, $c = 24.145(11)$ Å, $V = 1082.8(6)$ $Å^3$

Unfortunately, any attempt to integrate the intensity data to produce reliable data to refine the structure of grahampearsonite failed. Calculated powder X-ray diffraction d spacings (I %, d in Å) for grahampearsonite are reported in Table 2. In the synthetic analog of grahampearsonite, there are 22 sites [P(1)-P(4),

Table 2. Calculated powder X-ray diffraction d spacings (I %, d in Å) for grahampearsonite

hkl	I_{cal}	d_{calc}
110	28	4.735
112	10	4.408
115	10	3.381
200	**78**	**3.348**
201	**35**	**3.317**
202	**55**	**3.227**
203	**54**	**3.091**
008	**100**	**3.018**
120	**35**	**2.995**
211	15	2.972
204	17	2.928
122	29	2.907
213	25	2.807
117	28	2.788
205	**53**	**2.752**
214	14	2.683
206	9	2.574
215	17	2.545
207	5	2.403
221	6	2.356
119	22	2.334
223	8	2.271
127	5	2.261
208	17	2.242
300	16	2.232
301	12	2.223
224	5	2.204
303	9	2.151
128	8	2.126
311	6	2.109
209	11	2.093
312	5	2.086
219	10	1.998
227	20	1.952
230	20	1.857

Note: Calculated X-ray powder diffraction data according to the crystal structure obtained from single-crystal diffraction structure determination using the software VESTA (Momma and Izumi 2011).
The intensities of the seven strongest lines are in bold.

Table 1. Chemical composition of grahampearsonite expressed in oxide wt% and atoms per formula unit (apfu)

	Mean	Min.	Max.	S.D.		apfu
Na_2O	0.16	–	0.25	0.09	Na	0.01
K_2O	0.03	–	0.10	0.04	K	0.00
MgO	0.14	0.12	0.18	0.02	Mg	0.01
CaO	42.12	41.22	42.90	0.56	Ca	1.92
FeO	0.77	0.37	1.89	0.53	Fe	0.03
SiO_2	0.33	0.26	0.45	0.07	Si	0.01
P_2O_5	55.44	54.11	56.55	0.90	P	1.99
SO_3	0.35	0.19	0.52	0.10	S	0.01
Total	99.35	98.60	100.78	0.85		

Notes: Formula calculated based on anions = 7 apfu. S.D. = standard deviation (σ).

Table 3. Comparison of grahampearsonite with other synthetic and natural isostructural species

Mineral	Ideal Formula	Crystal System	Space Group	*a* (Å)	*c* (Å)	*V* (Å^3)	*Z*	Ref.
Grahampearsonite	$Ca_2P_2O_7$	Tet.	$P4_1$	6.6966(16)	24.145(11)	1082.8(6)	8	[0]
β-$Ca_2P_2O_7$	$Ca_2P_2O_7$	Tet.	$P4_1$	6.66	23.86	1058.3	8	[1]
		Tet.	$P4_1$	6.685	24.154	1079.4	8	[2]
		Tet.	$P4_1$	6.684	24.144	1078.7	8	[3]
		Tet.	$P4_1$	6.6858	24.147	1079.4	8	[4]
Percleveite-(Ce)	$Ce_2Si_2O_7$	Tet.	$P4_1$	6.7805	24.689	1135.1	8	[5]
Percleveite-(La)	$La_2Si_2O_7$	Tet.	$P4_1$	6.8482	24.8550	1165.64	8	[6]

Note: [0] This work; [1] Corbridge 1957; [2] Keppler 1962; [3] Webb 1966; [4] Boudin et al. 1993; [5] Holtstam et al. 2003; [6] Kasatkin et al. 2020.

Ca(1)-Ca(4), and O(1)-O(14)], that would require ~200 parameters to be refined, which in turn would require ~2000 unique reflections to produce a reliable structure refinement, far more than the 428 unique reflections integrated from the grahampearsonite inclusion. Even for an isotropic refinement, ~90 parameters would need to be refined, requiring ~900 unique reflections. Here, only 428 unique reflections were obtained, showing an average F2/sigma(F2) equal to only 1.10, which means that the average intensity of the collected reflections is extremely low and thus the number of reflections with sufficient intensity to be used for a structure refinement is actually much lower than 428. Moreover, in general, when one attempts to integrate reflections from a mineral still trapped within a diamond, some degree of "masking" must be applied to the reflections from the host diamond, which are extremely intense. This causes further reduction in the number of unique reflections from the inclusion that can be used in the structure refinement.

The unit-cell parameters obtained by single-crystal X-ray diffraction on grahampearsonite after the diamond polish are consistent, within experimental uncertainty, with those reported for synthetic β-$Ca_2P_2O_7$ (e.g., Corbridge 1957; Keppler 1962; Webb 1966; Cornilsen and Condrate 1979; Boudin et al. 1993; Bian et al. 2004), confirming the identification of grahampearsonite as the natural analog of β-$Ca_2P_2O_7$ (see Table 3). The close match of the measured unit-cell parameters with published values for β-$Ca_2P_2O_7$, combined with the Raman and FTIR results and with the WDS-EDS data, provides robust evidence for the natural occurrence of β-$Ca_2P_2O_7$, formally approved by the IMA-CNMNC as grahampearsonite. According to the structural model proposed by Boudin et al. (1993), the Ca atoms have different oxygen coordination numbers: Ca(1) and Ca(3) are 7-coordinated, Ca(2) is 9-coordinated, and Ca(4) is 8-coordinated. The P atoms are tetrahedrally coordinated by oxygen atoms forming $[P_2O_7]^{4-}$ groups, which are linked by Ca polyhedra (Fig. 6). The $[P_2O_7]^{4-}$ groups occur along (001) layers along with Ca polyhedra that link adjacent $[P_2O_7]^{4-}$ groups (see Online Materials[1] for the CIF).

Discussion

The identification of grahampearsonite as the natural analog of synthetic β-$Ca_2P_2O_7$ is strongly supported by micro-Raman, FTIR, crystal chemical, and X-ray diffraction data. The phase crystallizes in the tetragonal system [space group: $P4_1$ (#76)] with unit-cell parameters $a = 6.6966(16)$ Å, $c = 24.145(11)$ Å, and $V = 1082.8(6)$ Å^3, in close agreement with synthetic β-$Ca_2P_2O_7$. Grahampearsonite is isostructural with β-$Ca_2P_2O_7$ (Corbridge 1957; Keppler 1962; Webb 1966; Boudin et al. 1993), and with several lanthanide disilicates, including percleveite-(Ce) (Holtstam et al. 2003) and percleveite-(La) (Kasatkin et al. 2020) (Table 3).

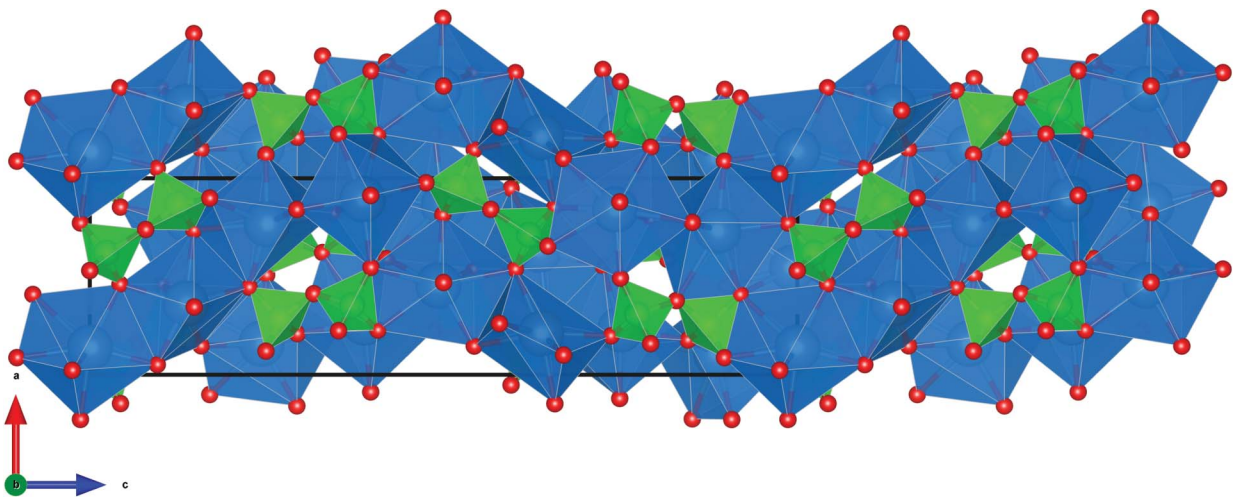

Figure 6. Crystal structure of grahampearsonite viewed along the **b** axis, modified after the synthetic β-$Ca_2P_2O_7$ described by Boudin et al. (1993). Phosphorus tetrahedra are shown in green, and Ca polyhedra are shown in blue. Coordinating oxygen atoms are shown in red. The unit cell is outlined with a solid black line. The structure was visualized using VESTA (Momma and Izumi 2011).

Grahampearsonite (β-$Ca_2P_2O_7$) has only been previously synthesized at ambient pressure and thus its occurrence as an inclusion in a sublithospheric diamond raises a question of whether it represents a high-pressure prograde or retrograde phase. Previous studies have demonstrated that β-tricalcium phosphate [β-TCP, β-$Ca_3(PO_4)_2$] can decompose into β-$Ca_2P_2O_7$ under specific conditions. Xu et al. (2006) observed this reaction in synthesized β-TCP, and de Fátima Gimenez et al. (2001) documented the formation of β-$Ca_2P_2O_7$ at the interface between β-TCP and $CaTi_4(PO_4)_6$ during high-temperature (>900 °C) treatment of phosphate-based glass-ceramics. Furthermore, synthesis experiments on β-TCP consistently report $Ca_2P_2O_7$ as a stable by-product when the bulk Ca/P ratio is below 1.5 (Ştefănescu and Stoia 2008).

Overall, these studies show that β-TCP could be partially decomposed into β-$Ca_2P_2O_7$. The coexistence of grahampearsonite with tuite [γ-$Ca_3(PO_4)_2$], the high-pressure polymorph of β-TCP, in RV43, suggests that during exhumation, tuite could be retrogressed and decomposed into a pyrophosphate phase. The preservation of β-$Ca_2P_2O_7$ in diamond provides natural evidence that $Ca_3(PO_4)_2$ polymorphs (i.e., tuite and β-TCP) may undergo retrogression, and highlights pyrophosphate phases as potential markers of the breakdown history of tuite in the deep mantle. Therefore, the coexistence of tuite and grahampearsonite in sample RV43 may record a two-stage history: high-pressure entrapment of tuite followed by lower temperature retrogression of tuite during ascent of the diamond host. The presence of tuite alone suggests sample RV43 formed at pressures of 7 GPa up to at least 15 GPa (Konzett and Frost 2009; Zhang et al. 2026), corresponding to depths down to ~450 km, within Earth's transition zone. Such estimates accord with other barometric work on inclusions in SDDs from the Juína region, which typically yield entrapment pressures of ~9–15 GPa (Anzolini et al. 2016, 2018, 2019; Brenker et al. 2021). However, recent works report tutite stabilized up to 25 GPa and 1700–1750 °C (Pausch et al. 2024), which would extend the depth of diamond formation to more than 700 km, in the lower mantle.

Implications

The occurrence of grahampearsonite in a SDD demonstrates that additional P-bearing phases are stable in the deep Earth, thereby extending the mineralogical record of the P cycle to the sublithospheric mantle. The majority of the P in oceanic and continental crust (~80 wt%, Walton et al. 2023) occurs in apatite. Previous studies describe how warm-slab subduction of oceanic crust, subsequent melting, and the production of carbonatitic melts in the upper mantle (up to the transition zone, Thomson et al. 2016), facilitate P-recycling due to the high compatibility of P in such melts (Baker and Wyllie 1992; Horton 2015). However, the occurrence of phosphate assemblages in SDDs suggests that in certain subduction systems, slab melting in the upper mantle is inhibited and P-bearing phases (e.g., apatite and its high-pressure polymorphs) are preserved and transported to the lower mantle. Experimental studies (Keshav and Gudfinnsson 2010; Kiseeva et al. 2013) have shown that for Ca-rich altered oceanic crust, the presence of calcite (or aragonite), rather than Na-carbonates, acts to depress the slab-solidus to lower mantle depths (Zhang et al. 2026). Therefore, in this type of Ca-rich oceanic crust, it is possible that P-bearing phases are transported to the transition zone or lower mantle, where they are eventually encapsulated during diamond growth. Such bulk compositions are documented by the occurrence of the Ca-bearing inclusion minerals, such as larnite, merrillite, apatite, diopside, and calcite in sample RV43 studied in this work. Zhang et al. (2026) suggest that such a Ca-rich composition may result from metasomatism of altered oceanic crust by Ca-rich fluids. Although more work is required to constrain the *P/T* phase relations of these Ca-phosphates, their use as tracers of deep P and C cycling in the deep Earth will surely be of critical importance in future studies on SDDs to investigate the deep Earth.

Acknowledgments and Funding

This study was funded by the Chinese Academy of Geological Sciences Basal Research Fund (JKYDM2025205) and Nest_Contratti_Ric_BIRD24_01, Department of Geosciences, University of Padova. It was also funded by the European Union (ERC, INHERIT, Starting Grant No.101041620). Views and opinions expressed are, however, those of the author(s) only and do not necessarily reflect those of the European Union or the European Research Council Executive Agency. Neither the European Union nor the granting authority can be held responsible for them. T.R.J., F.G., S.W.S., and R.A.F. acknowledge Conselho Nacional de Desenvolvimento Científico e Tecnológico research fellowships. We thank G. Redhammer and an anonymous reviewer for their comments.

References Cited

Angel, R.J., Alvaro, M., and Nestola, F. (2022) Crystallographic methods for non-destructive characterization of mineral inclusions in diamonds. Reviews in Mineralogy and Geochemistry, 88, 257–305, https://doi.org/10.2138/rmg.2022.88.05.

Anzolini, C., Angel, R.J., Merlini, M., Derzsi, M., Tokár, K., Milani, S., Krebs, M.Y., Brenker, F.E., Nestola, F., and Harris, J.W. (2016) Depth of formation of $CaSiO_3$-walstromite included in super-deep diamonds. Lithos, 265, 138–147, https://doi.org/10.1016/j.lithos.2016.09.025.

Anzolini, C., Prencipe, M., Alvaro, M., Romano, C., Vona, A., Lorenzon, S., Smith, E.M., Brenker, F.E., and Nestola, F. (2018) Depth of formation of super-deep diamonds: Raman barometry of $CaSiO_3$-walstromite inclusions. American Mineralogist, 103, 69–74, https://doi.org/10.2138/am-2018-6184.

Anzolini, C., Nestola, F., Mazzucchelli, M.L., Alvaro, M., Nimis, P., Gianese, A., Morganti, S., Marone, F., Campione, M., Hutchison, M.T., and others. (2019) Depth of diamond formation obtained from single periclase inclusions. Geology, 47, 219–222, https://doi.org/10.1130/G45605.1.

Baitahe, R., Sronsri, C., Thompho, S., Chaiseeda, K., Montri, N., and Boonchom, B. (2022) Correlation between structure, chromaticity, and dielectric properties of calcium copper pyrophosphates, $Ca_{2-x}Cu_xP_2O_7$. Scientific Reports, 12, 6869, https://doi.org/10.1038/s41598-022-11056-4.

Baker, M.B. and Wyllie, P.J. (1992) High-pressure apatite solubility in carbonate-rich liquids: Implications for mantle metasomatism. Geochimica et Cosmochimica Acta, 56, 3409–3422, https://doi.org/10.1016/0016-7037(92)90388-Y.

Bian, J.J., Kim, D.W., and Hong, K.S. (2003) Microwave dielectric properties of $Ca_2P_2O_7$. Journal of the European Ceramic Society, 23, 2589–2592, https://doi.org/10.1016/S0955-2219(03)00138-9.

Bian, J.J., Kim, D.W., and Hong, K.S. (2004) Phase transformation and sintering behavior of $Ca_2P_2O_7$. Materials Letters, 58, 347–351, https://doi.org/10.1016/S0167-577X(03)00498-1.

Bih, H., Saadoune, I., and Mansori, M. (2006) The lamellar $Na_2CoP_2O_7$ pyrophosphate: Preparation, structural and spectroscopic studies. Moroccan Journal of Condensed Matter, 7, 74–76.

Boudin, S., Grandin, A., Borel, M.M., Leclaire, A., and Raveau, B. (1993) Redetermination of the β-$Ca_2P_2O_7$ structure. Acta Crystallographica Section C, 49, 2062–2064, https://doi.org/10.1107/S0108270193005608.

Brenker, F.E., Nestola, F., Brenker, L., Peruzzo, L., and Harris, J.W. (2021) Origin, properties, and structure of breyite: The second most abundant mineral inclusion in super-deep diamonds. American Mineralogist, 106, 38–43, https://doi.org/10.2138/am-2020-7513.

Cabral-Neto, I., Ruberti, E., Pearson, D.G., Luo, Y., Azzone, R.G., Silveira, F.V., and Almeida, V.V. (2024) Diamond sources of the Juína region, Amazonian craton: Textural and mineral chemical characteristics of Kimberley-type pyroclastic kimberlites. Mineralogy and Petrology, 118, 1–22, https://doi.org/10.1007/s00710-023-00849-8.

Calvo, C. (1968) Crystal structure of α-$Ca_2P_2O_7$. Inorganic Chemistry, 7, 1345–1351, https://doi.org/10.1021/ic50065a019.
Corbridge, D.E.C. (1957) Crystallographic data on some hypophosphates and pyrophosphates. Acta Crystallographica, 10, 85, https://doi.org/10.1107/S0365110X57000201.
—— (1966) The structural chemistry of phosphorus compounds. In E.J. Griffith and M. Grayson, Eds., Topics in Phosphorus Chemistry, 3, p. 275. Wiley.
Cornilsen, B.C. and Condrate, R.A. Sr. (1979) The vibrational spectra of β-$Ca_2P_2O_7$ and γ-$Ca_2P_2O_7$. Journal of Inorganic and Nuclear Chemistry, 41, 602–605, https://doi.org/10.1016/0022-1902(79)80457-1.
Day, M.C., Pamato, M.G., Novella, D., and Nestola, F. (2023) Imperfections in natural diamond: The key to understanding diamond genesis and the mantle. La Rivista del Nuovo Cimento della Società Italiana di Fisica, 46, 381–471, https://doi.org/10.1007/s40766-023-00045-6.
de Fátima Gimenez, I., Mazali, I.O., and Alves, O.L. (2001) Application of Raman spectroscopy to the study of the phase composition of phosphate based glass-ceramics. Journal of Physics and Chemistry of Solids, 62, 1251–1255, https://doi.org/10.1016/S0022-3697(01)00017-8.
Elbashir, S., Broström, M., and Skoglund, N. (2024) Thermodynamic modelling assisted three-stage solid state synthesis of high purity β-$Ca_3(PO_4)_2$. Materials & Design, 238, 112679, https://doi.org/10.1016/j.matdes.2024.112679.
Genzel, P.-T., Pamato, M.G., Novella, D., Santello, L., Lorenzon, S., Shirey, S.B., Pearson, D.G., Nestola, F., and Brenker, F.E. (2023) Geobarometric evidence for a LM/TZ origin of $CaSiO_3$ in a sublithospheric diamond. Geochemical Perspectives Letters, 25, 41–45, https://doi.org/10.7185/geochemlet.2313.
Gras, P., Rey, C., Marsan, O., Sarda, S., and Combes, C. (2013) Synthesis and characterisation of hydrated calcium pyrophosphate phases of biological interest. European Journal of Inorganic Chemistry, 2013, 5886–5895, https://doi.org/10.1002/ejic.201300955.
Holtstam, D., Norrestam, R., and Andersson, U.B. (2003) Percleveite-(Ce)—A new lanthanide disilicate mineral from Bastnäs, Skinnskatteberg, Sweden. European Journal of Mineralogy, 15, 725–731, https://doi.org/10.1127/0935-1221/2003/0015-0725.
Horton, F. (2015) Did phosphorus derived from the weathering of large igneous provinces fertilize the Neoproterozoic Ocean? Geochemistry, Geophysics, Geosystems, 16, 1723–1738, https://doi.org/10.1002/2015GC005792.
Kaminsky, F.V. and Zedgenizov, D.A. (2022) First find of merrillite, $Ca_3(PO_4)_2$, in a terrestrial environment as an inclusion in lower-mantle diamond. American Mineralogist, 107, 1652–1655, https://doi.org/10.2138/am-2022-8175.
Kaminsky, F.V., Sablukov, S.M., Belousova, E.A., Andreazza, P., Tremblay, M., and Griffin, W.L. (2010) Kimberlitic sources of super-deep diamonds in the Juina area, Mato Grosso State, Brazil. Lithos, 114, 16–29, https://doi.org/10.1016/j.lithos.2009.07.012.
Kaminsky, F.V., Wirth, R., and Schreiber, A. (2013) Carbonatitic inclusions in deep mantle diamond from Juina, Brazil: New minerals in the carbonate-halide association. Canadian Mineralogist, 51, 669–688, https://doi.org/10.3749/canmin.51.5.669.
Kasatkin, A.V., Zubkova, N.V., Pekov, I.V., Chukanov, N.V., Škoda, R., Agakhanov, A.A., Belakovskiy, D.I., Ksenofontov, D.A., Plášil, J., Kuznetsov, A.M., and others. (2020) The mineralogy of the historical Mochalin Log REE deposit, South Urals, Russia. Part III. Percleveite-(La), $La_2Si_2O_7$, a new REE disilicate mineral. Mineralogical Magazine, 84, 913–920, https://doi.org/10.1180/mgm.2020.81.
Keppler, U. (1962) Synthetische Einkristalle von β-$Ca_2P_2O_7$. Die Naturwissenschaften, 49, 446–447, https://doi.org/10.1007/BF00632137.
Keshav, S. and Gudfinnsson, G.H. (2010) Experimentally dictated stability of carbonated oceanic crust to moderately great depths in the Earth: Results from the solidus determination in the system CaO-MgO-Al_2O_3-SiO_2-CO_2. Journal of Geophysical Research: Solid Earth, 115, B05205, https://doi.org/10.1029/2009JB006457.
Kiseeva, E.S., Litasov, K.D., Yaxley, G.M., Ohtani, E., and Kamenetsky, V.S. (2013) Melting and phase relations of carbonated eclogite at 9–21 GPa and the petrogenesis of alkali-rich melts in the deep mantle. Journal of Petrology, 54, 1555–1583, https://doi.org/10.1093/petrology/egt023.
Kohale, R.L. and Dhoble, S.J. (2012) Luminescence in Eu^{2+}-activated microcrystalline pyrophosphor. Micro & Nano Letters, 7, 453–455, https://doi.org/10.1049/mnl.2012.0173.
—— (2018) Optical performance of $Ca_2P_2O_7$:Ce^{3+} pyrophosphate phosphor synthesized via modified solid state diffusion. Journal of Molecular Structure, 1170, 18–23, https://doi.org/10.1016/j.molstruc.2018.05.065.
Konzett, J. and Frost, D.J. (2009) The high *P*–*T* stability of hydroxyl-apatite in natural and simplified MORB—An experimental study to 15 GPa with implications for transport and storage of phosphorus and halogens in subduction zones. Journal of Petrology, 50, 2043–2062, https://doi.org/10.1093/petrology/egp068.
Lin, F.H., Liaw, J.R., Hon, M.H., and Wang, C.Y. (1995) The effects of $Na_4P_2O_7{\cdot}10H_2O$ addition on the mechanical properties of sintered $Ca_2P_2O_7$ bioceramic. Materials Chemistry and Physics, 41, 110–116, https://doi.org/10.1016/0254-0584(95)01541-8.
Lorenzon, S., Wenz, M., Nimis, P., Jacobsen, S.D., Pasqualetto, L., Pamato, M.G., Novella, D., Zhang, D., Anzolini, C., Regier, M., and others. (2023) Dual origin of ferropericlase inclusions within super-deep diamonds. Earth and Planetary Science Letters, 608, 118081, https://doi.org/10.1016/j.epsl.2023.118081.
Miller, S.L. and Parris, M. (1964) Synthesis of pyrophosphate under primitive earth conditions. Nature, 204, 1248–1250, https://doi.org/10.1038/2041248a0.
Momma, K. and Izumi, F. (2011) VESTA 3 for three-dimensional visualization of crystal, volumetric and morphology data. Journal of Applied Crystallography, 44, 1272–1276, https://doi.org/10.1107/S0021889811038970.
Nestola, F., Zhang, Q., Day, M.C., Lorenzon, S., Pamato, M.G., Rocchetti, I., Bendazzoli, C., Novella, D., Mazzoli, C., Sassi, R., and others. (2025) RamanCrystalHunter: A new program and database for processing, analysis, and identification of Raman spectra. American Mineralogist, 110, 513–524, https://doi.org/10.2138/am-2024-9457.
Pausch, T., Joachim-Mrosko, B., Withers, A.C., Ludwig, T., Vazhakuttiyakam, J., and Konzett, J. (2024) The role of calcium phosphates and silicates in the storage and transport of phosphorus at the upper-to-lower mantle transition: An experimental study to 25 GPa in a model peridotitic bulk composition. Geochimica et Cosmochimica Acta, 374, 200–216, https://doi.org/10.1016/j.gca.2024.04.026.
Pearson, D.G., Brenker, F.E., Nestola, F., McNeill, J., Nasdala, L., Hutchison, M.T., Matveev, S., Mather, K., Silversmit, G., Schmitz, S., and others. (2014) Hydrous mantle transition zone indicated by ringwoodite included within diamond. Nature, 507, 221–224, https://doi.org/10.1038/nature13080.
Petrova, M.A., Shitova, V.I., Mikirticheva, G.A., Popova, V.F., and Malshikov, A.E. (1995) New data on $Zn_2P_2O_7$ phase transformations. Journal of Solid State Chemistry, 119, 219–223, https://doi.org/10.1016/0022-4596(95)80035-N.
Ranby, P.W., Mash, D.H., and Henderson, S.T. (1955) The investigation of new phosphors, with particular reference to the pyrophosphates. British Journal of Applied Physics, 6, S18–S24, https://doi.org/10.1088/0508-3443/6/S4/307.
Sauskojus, W., Wied, J.K., Litterscheid, C.F., Mangstl, M., and Schmedt auf der Günne, J. (2022) Crystal Structure of γ-$Ca_2P_2O_7$. Zeitschrift für Anorganische und Allgemeine Chemie, 648, e202200196, https://doi.org/10.1002/zaac.202200196.
Shirey, S.B., Pearson, D.G., Stachel, T., and Walter, M.J. (2024) Sublithospheric diamonds: Plate tectonics from Earth's deepest mantle samples. Annual Review of Earth and Planetary Sciences, 52, 249–293, https://doi.org/10.1146/annurev-earth-032320-105438.
Smith, E.M., Krebs, M.Y., Genzel, P.T., and Brenker, F.E. (2022) Raman identification of inclusions in diamond. Reviews in Mineralogy and Geochemistry, 88, 451–473, https://doi.org/10.2138/rmg.2022.88.08.
Sronsri, C. and Boonchom, B. (2018) Synthesis, characterization, vibrational spectroscopy, and factor group analysis of partially metal-doped phosphate materials. Spectrochimica Acta Part A: Molecular and Biomolecular Spectroscopy, 194, 230–240, https://doi.org/10.1016/j.saa.2018.01.034.
Stachel, T., Aulbach, S., and Harris, J.W. (2022) Mineral inclusions in lithospheric diamonds. Reviews in Mineralogy and Geochemistry, 88, 307–391, https://doi.org/10.2138/rmg.2022.88.06.
Ştefănescu, O.E., and Stoia, M. (2008) Preparation of β-tricalcium phosphate from precursors obtained by a wet precipitation method [articol]. Chemical Bulletin "POLITEHNICA" Univ. (Timişoara), 53, 204–207.
Thomson, A.R., Walter, M.J., Kohn, S.C., and Brooker, R.A. (2016) Slab melting as a barrier to deep carbon subduction. Nature, 529, 76–79, https://doi.org/10.1038/nature16174.
Walton, C.R., Ewens, S., Coates, J.D., Blake, R.E., Planavsky, N.J., Reinhard, C., Ju, P., Hao, J., and Pasek, M.A. (2023) Phosphorus availability on the early Earth and the impacts of life. Nature Geoscience, 16, 399–409, https://doi.org/10.1038/s41561-023-01167-6.
Warr, L.N. (2021) IMA-CNMNC approved mineral symbols. Mineralogical Magazine, 85, 291–320, https://doi.org/10.1180/mgm.2021.43.
Webb, N.C. (1966) The crystal structure of β-$Ca_2P_2O_7$. Acta Crystallographica, 21, 942–948, https://doi.org/10.1107/S0365110X66004225.
Xu, J.L., Khor, K.A., Kumar, R., and Cheang, P. (2006) RF induction plasma synthesized calcium phosphate nanoparticles. Key Engineering Materials, 309-311, 511–514, https://doi.org/10.4028/www.scientific.net/KEM.309-311.511.
Zhang, Q., Brenker, F.E., Timmerman, S., Shirey, S.B., Stachel, T., Luth, R.W., Locock, A.J., Stern, R.A., Chinn, I.L., Vincze, L., and others. (2026) Diamond evidence for limited subduction of phosphorus into the lower mantle. Geology, 54, 435–439, https://doi.org/10.1130/G54011.1.

Manuscript received October 19, 2025
Manuscript accepted November 28, 2025
Accepted manuscript online December 5, 2025
Manuscript Handled by G. Diego Gatta

Endnotes:

[1]Deposit item AM-26-610072. Online Materials are free to all readers. Go online, via the table of contents or article view, and find the tab or link for supplemental materials. The CIF has been peer-reviewed by our Technical Editors.